

A new photocrosslinkable polycaprolactone-based ink for three-dimensional inkjet printing

Yinfeng He,¹ Christopher J. Tuck,¹ Elisabetta Prina,² Sam Kilsby,³ Steven D. R. Christie,³ Stephen Edmondson,⁴ Richard J. M. Hague,¹ Felicity R. A. J. Rose,² Ricky D. Wildman¹

¹Faculty of Engineering, University of Nottingham, Nottingham, UK

²School of Pharmacy, Centre for Biomolecular Sciences, University of Nottingham, Nottingham, UK

³Department of Chemistry, Loughborough University, Loughborough, UK

⁴Department of Materials, University of Manchester, Manchester, UK

Received 25 November 2015; revised 8 April 2016; accepted 14 April 2016

Published online 14 May 2016 in Wiley Online Library (wileyonlinelibrary.com). DOI: 10.1002/jbm.b.33699

Abstract: A new type of photocrosslinkable polycaprolactone (PCL) based ink that is suitable for three-dimensional (3D) inkjet printing has been developed. Photocrosslinkable Polycaprolactone dimethylacrylate (PCLDMA) was synthesized and mixed with poly(ethylene glycol) diacrylate (PEGDA) to prepare an ink with a suitable viscosity for inkjet printing. The ink performance under different printing environments, initiator concentrations, and post processes was studied. This showed that a nitrogen atmosphere dur-

ing printing was beneficial for curing and material property optimization, as well as improving the quality of structures produced. A simple structure, built in the z-direction, demonstrated the potential for this material for the production of 3D printed objects. Cell tests were carried out to investigate the biocompatibility of the developed ink. © 2016 The Authors Journal of Biomedical Materials Research Part B: Applied Biomaterials Published by Wiley Periodicals, Inc. J Biomed Mater Res Part B: Appl Biomater, 105B: 1645–1657, 2017.

How to cite this article: He Y, Tuck CJ, Prina E, Kilsby S, Christie SDR, Edmondson S, Hague RJM, Rose FRAJ, Wildman RD. 2017. A new photocrosslinkable polycaprolactone-based ink for three-dimensional inkjet printing. J Biomed Mater Res Part B 2017;105B:1645–1657.

INTRODUCTION

The need for biodegradable materials for health care applications has stimulated interest in the development of bioresorbable polymer materials. A range of materials have been considered for these applications, including polycaprolactone (PCL), poly(lactic acid), and other aliphatic polyesters.^{1–3} Of particular interest is PCL, which is able to decompose through random hydrolytic chain scission of its ester groups.^{4,5} PCL is a biodegradable and semicrystalline polymer, with a relatively long degradation period⁶ making it suitable for implant-based drug delivery applications. Bioresorbable drug-impregnated polymer systems are able to release therapeutic agents to the environment, and if one is able to incorporate the dose in a controlled manner, this could potentially lead to new, personalizable treatments.^{7–9}

Additive manufacturing (AM) [or three-dimensional (3D) printing] is a disruptive technology that can produce a 3D object based on digital design data through the sequential addition of layered materials.¹⁰ This process presents significant advantages over traditional manufacturing methods since one is able to personalize with little marginal unit cost. The design freedoms that are realized by AM enable greater

flexibility and as a consequence greater value of the final product.¹¹ This technology has developed from a purely prototyping nature, to one set for the production of objects that can see their life in service. To date, the bespoke nature of AM has enabled use in areas, such as prosthetics and bone replacement.^{12–15} Benefits have been sought in the reconstruction of anatomical structures^{16–19} and for porous implants with interconnecting fenestration for bone growth.^{20,21} If such benefits were combined with bioresorbability and drug delivery, then a significant step change in treatment could be achieved. In this context, PCL for AM production of health care products has already been recognized. Early attempts have been made to use it as a build material for powder bed fusion, material extrusion techniques, and stereolithography.^{12–14,22,23} However, for advanced structures that may contain more than one material, there is a need to control the discrete deposition of each material with high resolution. Although it is possible, powder bed fusion and material extrusion have significant difficulties in the production of multimaterial, high-resolution products.

An alternative technique is inkjet-based 3D printing to produce two-dimensional and 3D structures.^{24–28} This technique

Correspondence to: Y. He; e-mail: ezzyh2@nottingham.ac.uk

This is an open access article under the terms of the Creative Commons Attribution License, which permits use, distribution and reproduction in any medium, provided the original work is properly cited.

allows the co-deposition of more than one material due to the possibility of multiple deposition heads.²⁹ The realization of an inkjet printable PCL-based ink, therefore, offers an increased potential for functionality in biomaterials' development and drug delivery systems through the high-resolution and multi-material deposition offered by material jetting.

The key step in inkjet based 3D printing is the conversion of the liquid ink to a useful solid. Photocrosslinking is one technique that is used and has seen commercialization for example in the Stratasys Connex and 3D Systems Polyjet machines.³⁰ PCL itself is not photocrosslinkable but has the potential to be modified into a photocurable polymer^{31,32} and, in addition, has been shown to retain the biodegradability of PCL,³³ leading to its consideration as a candidate as an inkjet based 3D printing material. This photocrosslinkable PCL has been shown to be processable using stereolithography,^{22,23} offering its use as a AM material, but in this work, the focus is on developing it as a base formulation for inkjet based 3D printing to create a platform material for multi-functional, graded structures in the future. To demonstrate the suitability of the material for inkjet printing, the methodology used to create and study the performance of different ink formulations will first be presented; subsequently it will be shown that a 3D solid structure can be formed.

MATERIALS AND METHODS

Material synthesis

3D inkjet printing requires a relatively low viscosity ink for jetting, but in order to form 3D structures, the printed ink needs to be able to solidify or cure quickly following deposition to prevent spreading.³⁴ A method of inducing curing is the use of Ultraviolet (UV) light.³⁵ UV curable materials normally contain certain photoreactive groups, such as acrylate and methyl acrylate, which can cross-link under UV light.³⁶ However, PCL does not contain these chemical moieties and, therefore, cannot be directly photocured. It has been shown that by attaching photoreactive groups onto a PCL polymer or oligomer chain, photocrosslinking is possible.³⁷ Here, in this study, methacrylate groups were used, leading to the production of PCL dimethylacrylate (PCLDMA), which was synthesized by a method based on that proposed by Feng and Zhao.

The production of the PCLDMA proceeded in the following way. A round bottomed flask was flame dried and filled with anhydrous tetrahydrofuran, 100 mL (anhydrous, $\geq 99.9\%$, inhibitor free; Sigma-Aldrich), PCL-dio, 110 mL, 20.2 mmol (average Mn ~ 530 ; Sigma-Aldrich), and dried triethylamine, 8.46 mL, 60.7 mmol ($\geq 99\%$; Sigma-Aldrich) in a nitrogen environment. The flask was then cooled to 0°C. Methacryloyl chloride 5.92 mL, 60.7 mmol ($\geq 97.0\%$ (GC), contains $\sim 0.02\%$ 2,6-di-tert-butyl-4-methylphenol as a stabilizer) was then added slowly within an 1-hour period using an automatic syringe pump. The reaction occurred over 17 hours and was then warmed back to room temperature. The residual solvent was removed using a rotary evaporator, after which diethyl ether 100 mL (laboratory; Fisher Scientific) was added and then stirred for 15 minutes. The mixture was settled and separated. The organic layer was extracted by a separator funnel and dried in a vacuum oven to remove volatiles. Fourier trans-

form infrared spectroscopy (FTIR) and Nuclear Magnetic Resonance (NMR) spectra were obtained to verify the formation of PCLDMA using a Bruker Tensor FTIR and Bruker AV(III) 500 MHz NMR spectrometer.

Ink preparation

Based on the measured viscosity and suggested range for the printhead, a diluent was required to reduce the viscosity to a range that was printable (Figure 1). In this case, poly(ethylene glycol) diacrylate (PEGDA) was used, which is a commonly used photocrosslinkable biocompatible material.³⁸⁻⁴⁰ Though not an aspect investigated here, it was noted that PCL is hydrophobic and PEG is hydrophilic, and any copolymers may have useful tunable properties.^{41,42}

The viscosity (under a shear rate of 1000 s^{-1}) was measured by a cone and plate rheometer (Malvern Kinexus Pro) under varying compositions. This was then used to identify diluent proportion and the processing temperature. Each measurement started at 25°C and proceeded with 5°C increments up to a maximum of 60°C. A protocol of waiting 300 seconds after reaching the test temperature was used to ensure that the ink was in a steady-state condition before measurement was taken. At each temperature point and shear rate, the viscosity was recorded at 5 second intervals within a 180 seconds testing time.

PCLDMA and PEGDA (average Mn ~ 250 ; Sigma-Aldrich) were mixed together in an 8-mL amber vial and stirred at room temperature for 15 minutes at 800 rpm (IKA RCT Basic IKAMAG Magnetic Stirrer with Temperature Controller). Photoinitiator (PI) (2,4-diethyl-9H-thioxanthen-9-one, 98%; Sigma-Aldrich) and accelerator (AC) (ethyl 4-(dimethylamino)benzoate, 99%; Sigma-Aldrich) were added into the PCLDMA:PEGDA mixture and stirred at room temperature until all the solutes were fully dissolved. Before printing, the prepared ink required degassing to remove dissolved oxygen to help minimize oxygen inhibition brought about by the presence of oxygen.^{43,44} The degassing procedure was carried out by purging the ink with nitrogen gas for 15 minutes, though this procedure created significant nitrogen bubbles formation within the ink, reducing the reliability of droplet formation during printing; as a consequence, to allow

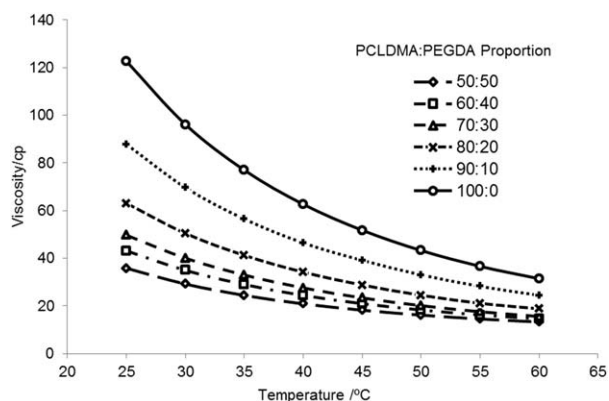


FIGURE 1. Viscosity distribution plot of PCLDMA:PEGDA with different proportions between 25 and 60°C at shear rate of 1000 s^{-1} .

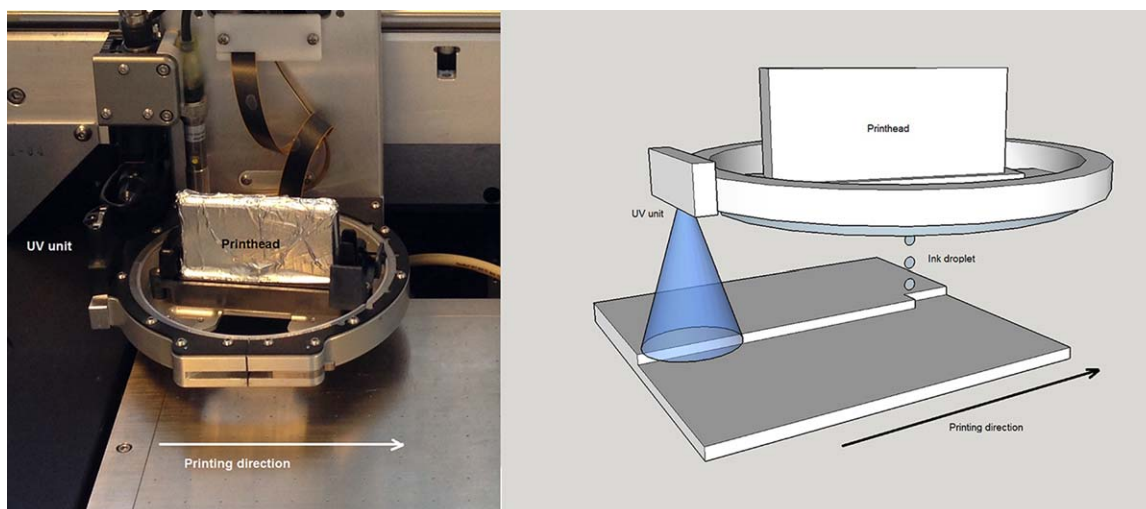


FIGURE 2. Structure and schematic of Dimatix printing unit and real-time curing.

the bubbles to disperse, the ink was allowed to settle overnight before printing.

The molecular weight of synthesized PCLDMA was determined by using size exclusion chromatography (Varian PL-GPC50). DMF (0.1 Wt % LiBr) was used as the eluent with a flow rate of 1 mL min^{-1} at 50°C .

Jetting and curing

Following ink preparation, $\sim 2 \text{ mL}$ of ink was injected into a 10-pL drop volume Dimatix cartridge and printed with a Dimatix DMP-2830 material printer. The ink-filling procedure was performed in the dark to prevent light being incident on the ink thus inducing curing; careful attention was also paid to handling to avoid bubble formation within the ink. To avoid any curing inside the cartridge during printing due to ambient light, the cartridge was wrapped with foil tape.

Curing was achieved by a UV unit (365 nm and 300 mW cm^{-2}) mounted directly on to the printing unit (Figure 2) allowing it to move with the printhead and induce real-time UV illumination and curing.

Characterization

An additional UV unit (365 nm and 100 mW cm^{-2}) was used to study the influence of different postcuring time (10, 20, and 30 minutes) on the mechanical properties of the printed parts. The printed samples were placed under the UV unit with the upper surface exposed.

Further experiments were carried out to investigate the influence of different PI concentrations as well as the printing environments on the final properties of the printed specimens. Inks with 1, 2, and 3 Wt % of PI and AC were prepared and printed following the same protocol in both air and nitrogen environments.

The mechanical properties of the printed samples were characterized by nanoindentation at room temperature (Micro Materials, NanoTest NTX with hot stage and inert gas cabinet). Both the top and bottom surfaces were characterized using a 5×5 grid of indentations with $100 \mu\text{m}$ sep-

aration between each. The peak force was set to 5 mN with a 0.25 mN s^{-1} loading and unloading rates. A spherical indenter with $50 \mu\text{m}$ radius was used. FTIR measurements were also carried out in attenuated Total Reflectance (ATR) mode (Bruker Tensor-27) with 2 cm^{-1} interval to track the curing of the printed samples. Printed mesh structures were sputter coated with platinum and examined by Scanning Electron Microscope (SEM) (XL30 ESEM Philips). The transmission spectrum of the printed ink with different amount of layers was printed onto quartz slides and characterized by UV-visible spectrophotometry.

Biocompatibility test. Biocompatibility was tested using both indirect and direct methods to assess any cytotoxic effects from any chemicals leaching out of the cured ink and to assess initial cell adhesion, respectively. A biocompatibility test was performed following the method of Elomaa et al.²² A sample was immersed in acetone for 20 hours to remove any unreacted polymer residuals and dried under vacuum until the weight was constant. The printed specimens were then sterilized by immersion in 70% (w/v) ethanol in deionized H_2O that was allowed to evaporate overnight under laminar flow. The samples were washed with phosphate-buffered saline (PBS) (Invitrogen) three times for 15 minutes²² and then incubated in $500 \mu\text{L}$ of the culture media for 72 hours at 37°C , 5% CO_2 in air. The media were then collected and labeled as “media extract.”

NIH3T3 fibroblasts were grown in Dulbecco’s modified eagle medium (Sigma-Aldrich) supplemented with 10% (v/v) of fetal bovine serum, 2 mM L-glutamine (Sigma-Aldrich), and 1% (v/v) gentamicin/amphotericin B (Sigma-Aldrich) at 37°C , 5% CO_2 in air. Once cells were 80%–90% confluent, cells were detached from the culture surface by using trypsin solution (0.025% trypsin and 0.01% ethylenediaminetetraacetic acid in PBS) and resuspended in culture media at a concentration of $8 \times 10^4 \text{ cells mL}^{-1}$. The cell suspension ($100 \mu\text{L}$) was then transferred into a 96-well plate and allowed to adhere for 24 hours at 37°C , 5% CO_2 in air.

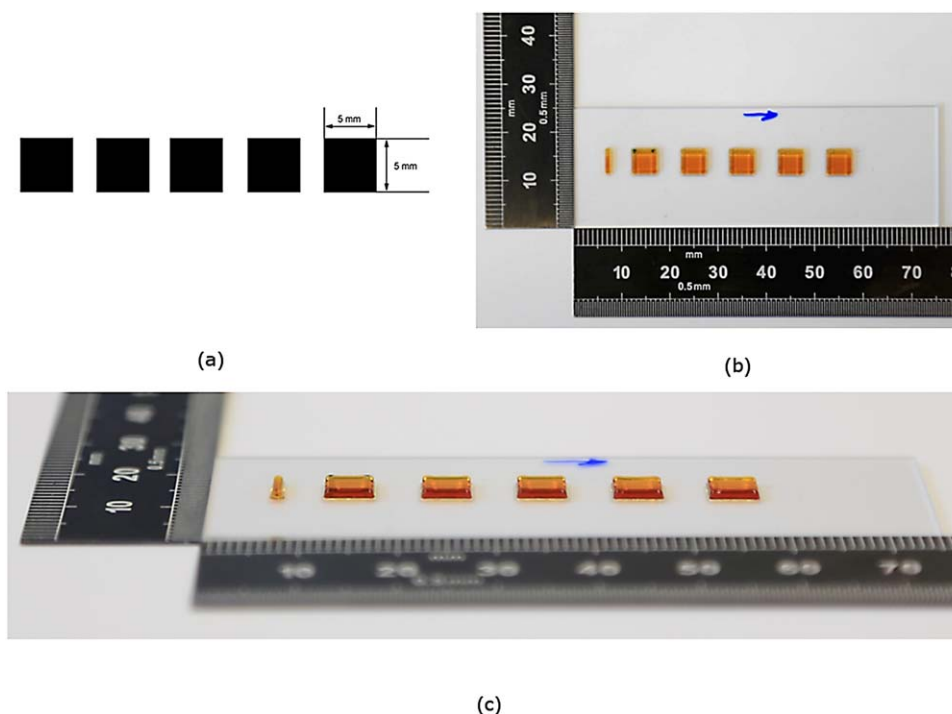


FIGURE 3. Printed square samples for nanoindentation test: (a) printing pattern, (b) top view, and (c) side view.

The culture media were then replaced with 200 μL of the “media extract,” and the cells incubated further over a period of 24 hours. Cell viability, using the PrestoBlue[®] assay was evaluated after day 1 and then tracked at day 3 and 5 with fresh media. Cells cultured in fresh culture media were considered as a positive control. PrestoBlue[®] (Invitrogen), a resazurin-based solution, was used to determine the metabolic activity of cells. It was performed according to the manufacturer’s protocols. In brief, a solution of 10% (v/v) of PrestoBlue[®] in cell culture media was prepared, and 100 μL was added to each well. After 45 minutes of incubation at 37°C, 90 μL of the assay solution was transferred to a 96-well plate (Corning), and the fluorescence intensity was evaluated using a spectrofluorometer (Tecan Infinite M200 microplate reader) at 560/590 nm. The percentage of viability was calculated as a ratio of that determined from the positive control. Five samples per each condition were considered.

A direct test was performed to evaluate metabolic activity of cells directly in contact with the scaffolds. The samples, after 72 hours of immersion in culture media, were seeded with 500 μL of cell suspension (at a density of 4×10^5 cells mL^{-1}). A negative control was created with the same conditions but without the addition of cells. After 24 hours, the scaffolds were moved to a new 48-well plate. The activity of the cells was evaluated by PrestoBlue[®] after 1, 3, and 5 days as described earlier. Five samples were evaluated for each condition.

Indirect and direct cytotoxicity data at different time points were presented as mean \pm standard error and compared using one-way ANOVA followed by a Tukey post hoc

test using Prism 6 (GraphPad Software, v6.01). A value of $p < 0.05$ was considered significant.

RESULTS

Synthesis of PCLDMA

The FTIR spectra of PCLDMA showed absorption band at 1637 and 810 cm^{-1} , which represents the C=C due to methyl acrylation of the PCL diol. The formation of PCLDMA was also confirmed by using ¹H NMR spectrometer and the C=C groups appeared in the δ 5.5–6.2 ppm range (figure not shown). Both results are comparable to the characterization results of photocrosslinkable PCLDA synthesized by Kweon et al.³³ The molecular weight of the synthesized PCLDMA was measured by GPC and found to be $M_n \sim 1683$ g mol^{-1} .

Real-time curing and postcuring effects

Five square specimens, 5 mm \times 5 mm, were printed with real-time photocrosslinking to investigate how the real-time photocrosslinking and postcuring processes will influence the sample’s properties. The specimens were created with 100 layers of ink, corresponding to depths of ~ 500 μm (shown in Figure 3).

The hardness and indentation modulus of the top and bottom surfaces of the printed samples as a function of postcuring time were measured using nanoindentation. It was anticipated that as the samples were produced by stacking up layers of material, with differing amounts of UV illumination for different layers, that this would lead to depth-dependent curing level and therefore depth-dependent properties.⁴⁵ What was observed, however, was that the top and bottom surfaces of the sample had very similar properties prior to

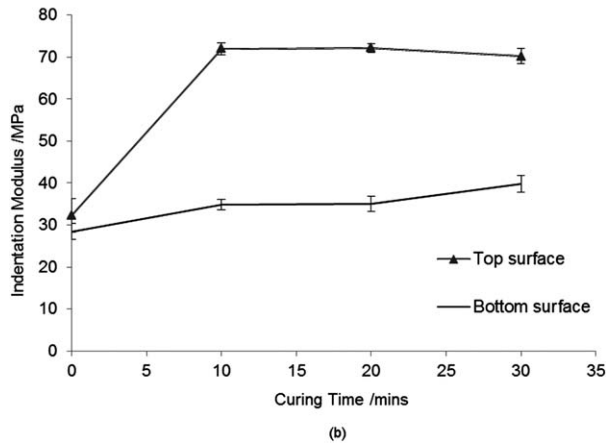
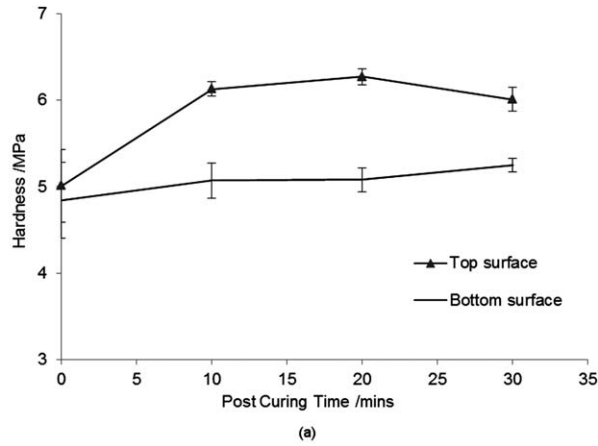


FIGURE 4. Plots of nanoindentation data for samples with different postcuring time: (a) hardness and (b) indentation modulus, olds. Data presented as mean ± standard error ($n = 4$).

any postcuring treatment, suggesting that the ink with 3 Wt % PI and AC allowed homogenous curing throughout the depth of the sample (Figure 4, 0 minute). Following postcuring, the sample's top surface showed a manifest increase in hardness and modulus. In contrast, the properties of the sam-

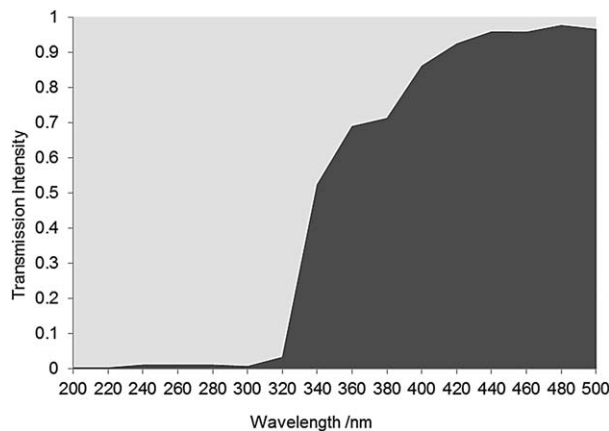


FIGURE 5. Transmission spectrum for one layer of printed PCLDMA:-PEGDA ink with 3 Wt % photoinitiator and accelerator in air environment.

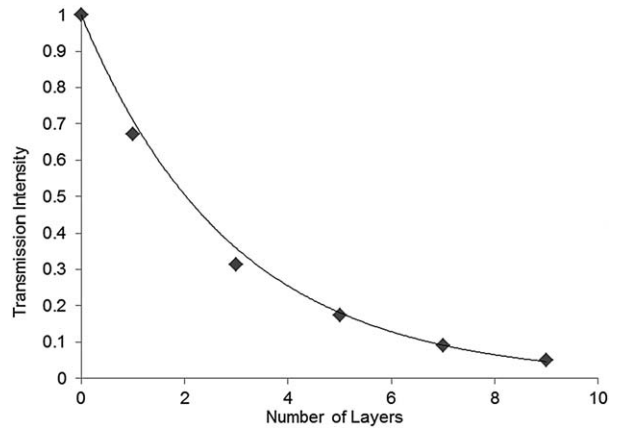


FIGURE 6. Plot of transmission change at 365 nm with increment in printed layers for PCLDMA:PEGDA ink with 3 Wt % photoinitiator and accelerator printed in air environment.

ple's bottom surface did not show a notable change with an increasing postcuring time.

The transmission spectrum of one printed and cured layer of ink was measured within a wavelength range between 200 and 500 nm (Figure 5). A further experiment was carried out to measure the transmission of three, five, seven, and nine layers of printed and cured ink at the wavelength of 365 nm, which was the UV wavelength used for curing. From Figure 6, it can be seen that a nine-layer sample's transmission was ~5%, while for one-layer sample's transmission was ~67.2%. Based on the Beer-Lambert law, the transmission of the light can be determined from the following equation:

$$T = \frac{I}{I_0} = e^{-\epsilon l} = e^{-\sigma Nt} \tag{1}$$

where T is the transmittance, I_0 is the incident radiation, I is the transmitted radiation, ϵ is the attenuation coefficient, σ is the attenuation cross section, l is the distance the light travelled, N is the number of sample layers, and t is the single layer thickness. Therefore, an exponential approach to full absorption was fitted (Figure 6):

$$T = e^{-0.342N} \tag{2}$$

Equation (2) can be used to calculate a characteristic skin depth over which the transmission decreased to an appreciable level, in this case $N = 2.92 \approx 3$ layers.

PI concentration and printing environment

Further experiments were carried out to investigate how various concentrations of PI and AC influence sample properties in both air and nitrogen environments. Inks with 1, 2, and 3 Wt % of PI and AC were prepared following the same procedure as before and printed. Square samples consisting of 100 printed layers were prepared for each ink in both air and nitrogen environments.

Morphology variations were observed for specimens printed with different inks in both environments (Figure 7).

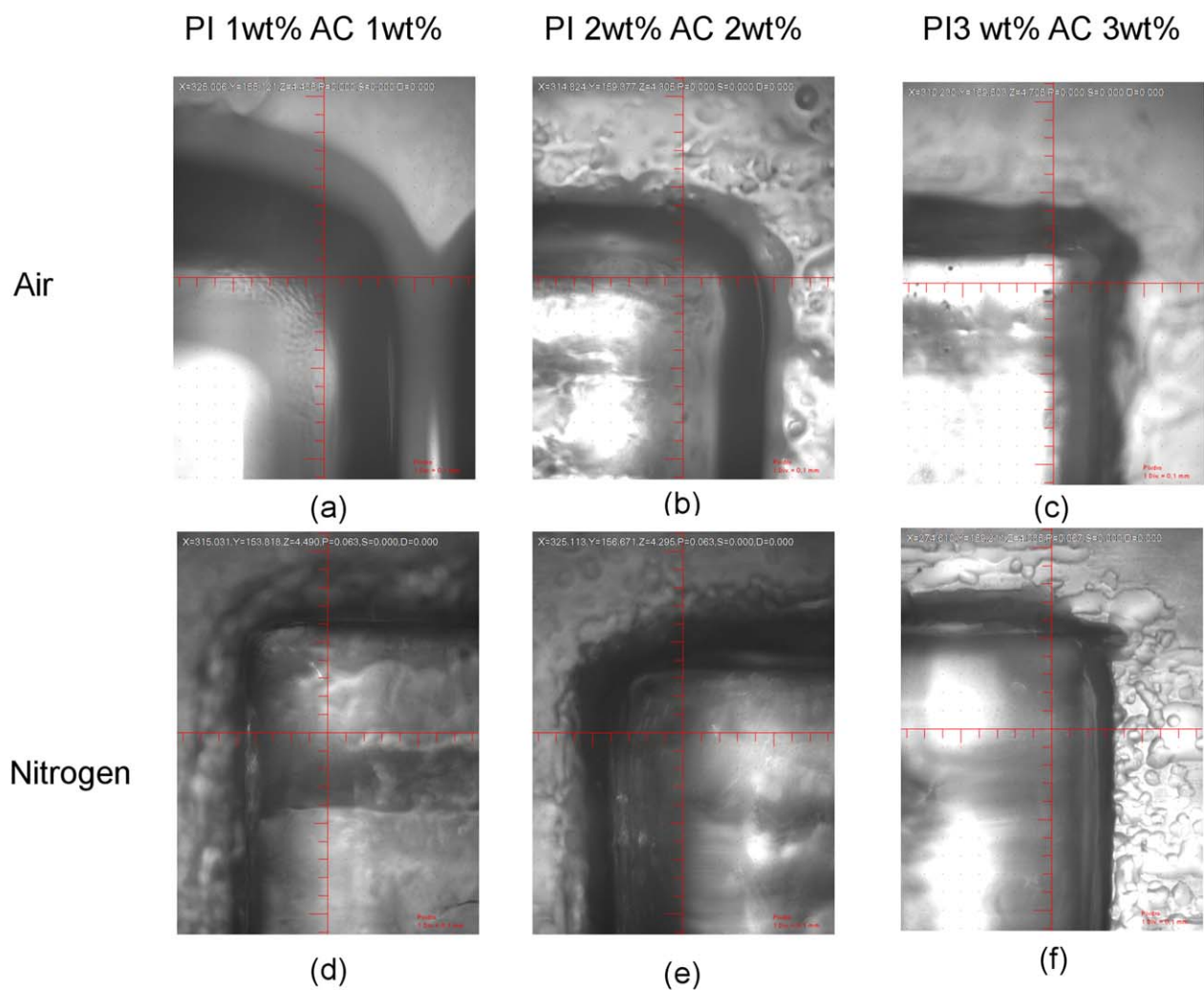


FIGURE 7. Optical microscope pictures of square samples printed with the inks containing different concentrations of PI and AC in both air and nitrogen environments (1 division = 100 μm).

For the ink with 1 Wt % PI and AC, the printed square samples present as rounded rectangular shapes after being printed in air [Figure 7(a)]. But the same ink produced sharp edges and corners when printed in nitrogen [Figure 7(d)].

The hardness and modulus of these samples were measured by nanoindentation tests on both surfaces following the same protocol established previously. The results are shown in Figures 8 and 9. For the samples printed in air, both the hardness and modulus of the top surface showed an upward trend with PI and AC concentration increases. This implies that lower PI and AC concentration will affect the curing speed when the ink is printed in air. FTIR characterization was carried out on both the surfaces of the printed samples in order to track the curing level of the deposited material (Figure 10).

Printing trials and characterization

Mesh structures [Figure 11(a)] of three different wall thicknesses (150, 300, and 500 μm) were printed and then examined with a SEM. The distance between each wall was set as 1 mm to allow each printed vertical or horizontal

wall to be separated from each other. Ten layers of PCLDMA:PEGDA (70:30) were printed, and the sample appearance is shown in Figure 11(b).

Figure 12 shows that under an air environment, the PCLDMA:PEGDA (70:30) ink could not form precise, sharp edges. Rectangular gaps were designed inside the mesh structure. However, in the actual printed structure, the rectangular shaped gap became rounded. Meanwhile, sagging of printed ink droplets could be observed from the SEM pictures and caused rounded rectangular gaps as well as curved walls. These may be due to the insufficient curing. The UV illumination unit was attached and moved with the printhead (Figure 1); therefore, the energy provided within a single scan may not have been sufficient to allow freshly deposited ink to become fully cured immediately. Without full curing, sagging due to gravity or movement of the platform may occur, leading to rounded edges and curved walls. This effect becomes more obvious when producing samples with small features.

However, as the illumination area of the UV unit was larger than the printed area of each printing cycle (as shown in the schematic representation of Figure 1), the

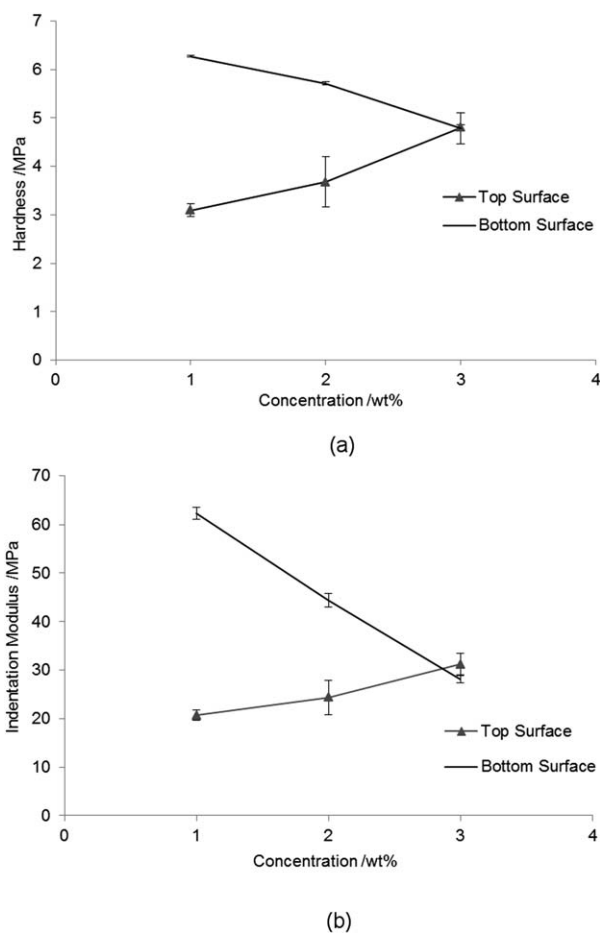


FIGURE 8. Plot of the top and bottom surface properties of the square samples printed in air environment by PCLDMA:PEGDA (70:30) with 1, 2, and 3 Wt % photoinitiator and accelerator: (a) hardness and (b) indentation modulus. Data presented as mean \pm standard error ($n = 4$).

previously deposited ink can still receive UV illumination during the following the printing of subsequent droplets. Therefore, the ink will receive intermittent UV illumination and will be finally cured once exposed to sufficient photons, although the curing time will be greater than would be found for continuous UV illumination. Increasing the curing speed could also help the printed ink cure in a shorter period of time, hence reduce the chance of sagging and improving the print quality. This could be achieved by either increasing the intensity of UV illumination, creating an oxygen-free environment or support material could be printed simultaneously around the structure to help restrict the sagging effect.

Figure 13 shows a printed curving mesh structure with PCLDMA:PEGDA (70:30) ink, which demonstrates the capability of the developed ink to create complex structures. Fifty layers were printed, and surface profiling data [Figure 13(d)] show that the total height of the structure was $\sim 250 \mu\text{m}$. Figure 14 shows optical microscopy images of a printed curving mesh structure. It was also observed in these samples that the ink did not fully cure immediately after deposition, and some of the droplets at the edges

slipped down to the substrate forming coarse structures at the base. Currently, this photocrosslinkable PCL-based ink has been used to form structures down to $200\text{--}300 \mu\text{m}$ in x - and y -axes, which could reach $50\text{--}100 \mu\text{m}$ if co-printing supports and printheads with smaller orifices were used. This makes it a competitive candidate to produce 3D-printed polymeric biomaterials.

Printing accuracy and resolution

In order to investigate the printing accuracy and resolution of the developed ink, line structures with different widths, number of layers, and gaps were printed and characterized with an optical microscope. Figure 15(a) compares the intended line width with the observed width, showing that when attempting to print on length scales near to a single droplet, differences of the order of a factor of two are observed, but at $10\times$ this scale, the differences drop to $\sim 10\%$. The dependence of the feature size on the number of layers was also tested. This indicated that although there was some spreading and growth, it was small and once again, if supporting structures were used, could be limited even further [Figure 15(b)]. The smallest separation of structures observable was $\sim 39 \mu\text{m}$, suggesting a resolution in the order of a droplet diameter.

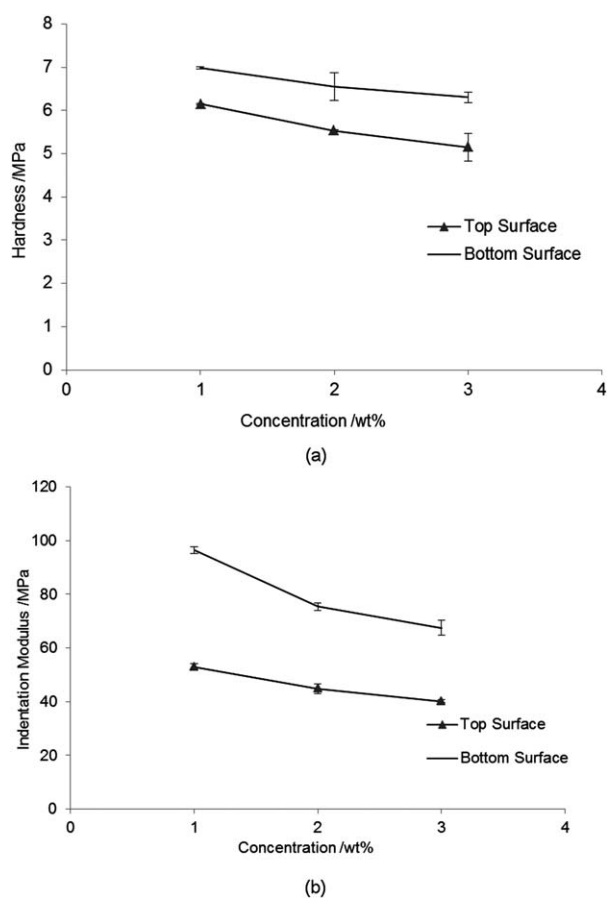


FIGURE 9. Plot of the top and bottom surface of the square samples printed in nitrogen environment by PCLDMA:PEGDA (70:30) with 1, 2, and 3 Wt % photoinitiator and accelerator: (a) hardness and (b) indentation modulus. Data presented as mean \pm standard error ($n = 4$).

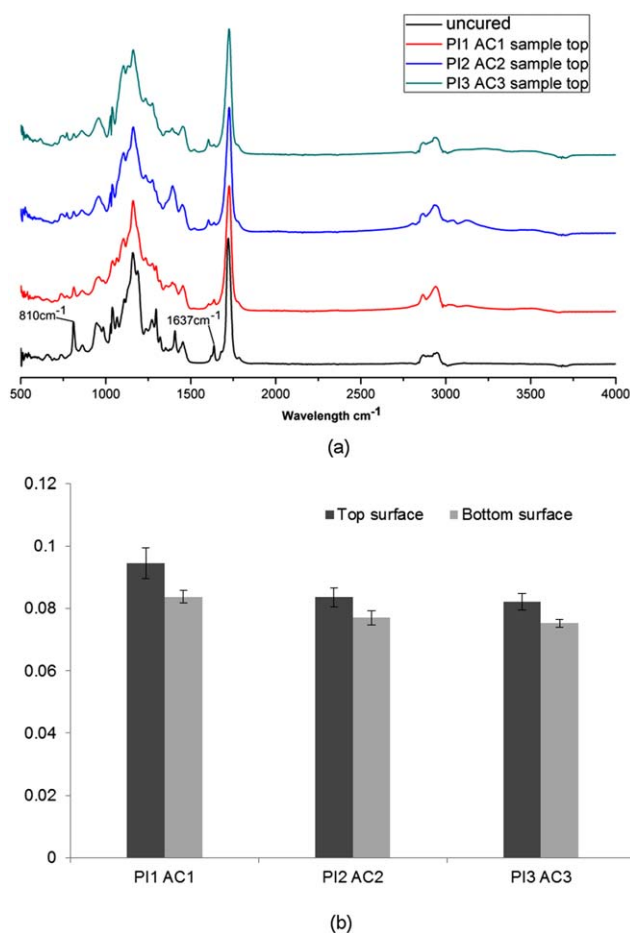


FIGURE 10. FTIR result of inks with different photoinitiator and accelerator concentrations printed in air environment: (a) FTIR results of the samples' top surface, (b) comparison of 810 cm^{-1} peak intensity. Data presented as mean \pm standard error ($n = 4$)

Biocompatibility of the photocrosslinked ink

The results of the biocompatibility experiments are shown in Figures 16 and 17. The PrestoBlue[®] assay is an indirect measure of cellular metabolic activity and was used to assess if any cytotoxic chemicals leached from the materials

and also to assess the ability of the cells to adhere to the samples. In the cytotoxicity experiment, the percentage viability as compared to a control (cells cultured on tissue culture plastic) was 60% after day 1, which then increased to 77% after day 3 and to 95% after day 5, suggesting that cells proliferated following exposure to the media extract, and so any initial cytotoxicity was overcome by the cells.

The metabolic activities of cells seeded on scaffolds in the direct compatibility test were evaluated after days 1, 3, and 5. After day 1, an elevated fluorescence signal indicated that cells adhered to the sample. On subsequent test days, at days 3 and 5, further increases in fluorescence suggest proliferation and viability on the cured ink.

DISCUSSION

This work aimed to demonstrate a developed photocrosslinkable PCL-based ink that is suitable for 3D inkjet printing to produce biocompatible 3D structures. During the investigation of the influences of processing parameters on the product properties, it was noticed that when the printed samples were subjected to further UV illumination (postcuring), a marked difference in the properties on the upper and lower surfaces was observed. The mechanical properties of the sample's top surface, which was directly illuminated by UV light, increased considerably after 10 minutes of postcuring (Figure 4). However, additional postcuring for 20 and 30 minutes did not further influence these properties. This suggested that the cross-linking density induced by the UV light has been almost saturated and no further cross linking occurred.^{46,47} When a specimen was printed, the conversion of the C=C group into the covalent cross-link was not likely to reach 100%, but the UV illumination during postprocessing can help convert the remaining C=C groups to form new cross-links and enable the material to reach its higher stiffness. During the postcuring procedure, samples were illuminated from the top surface, and the UV irradiation needs to penetrate the whole sample before reaching the bottom surface. The apparent homogeneity in the mechanical properties and the subsequent difference when subjected to intense radiation from above mean that each layer was able to partially cure to the same degree

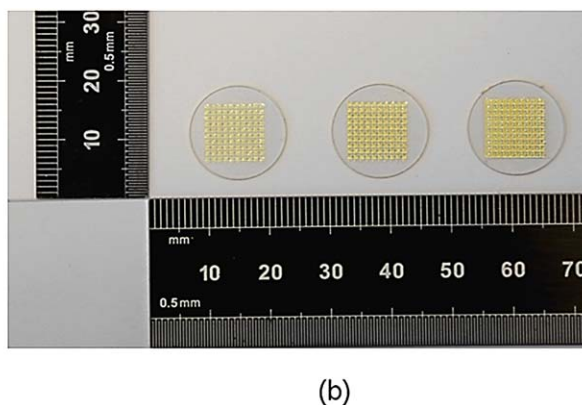
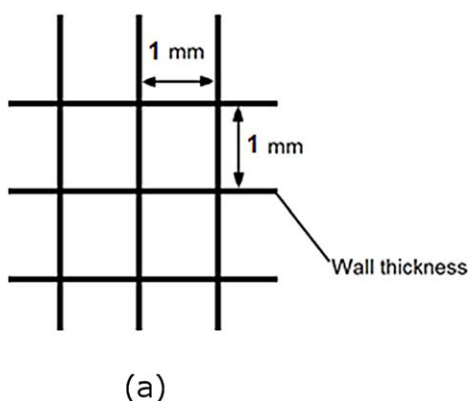


FIGURE 11. Printed mesh samples for processing accuracy check. (a) Schematic diagram of printing pattern design and (b) printed sample with different wall thickness (150, 300, and 500 μm from left to right).

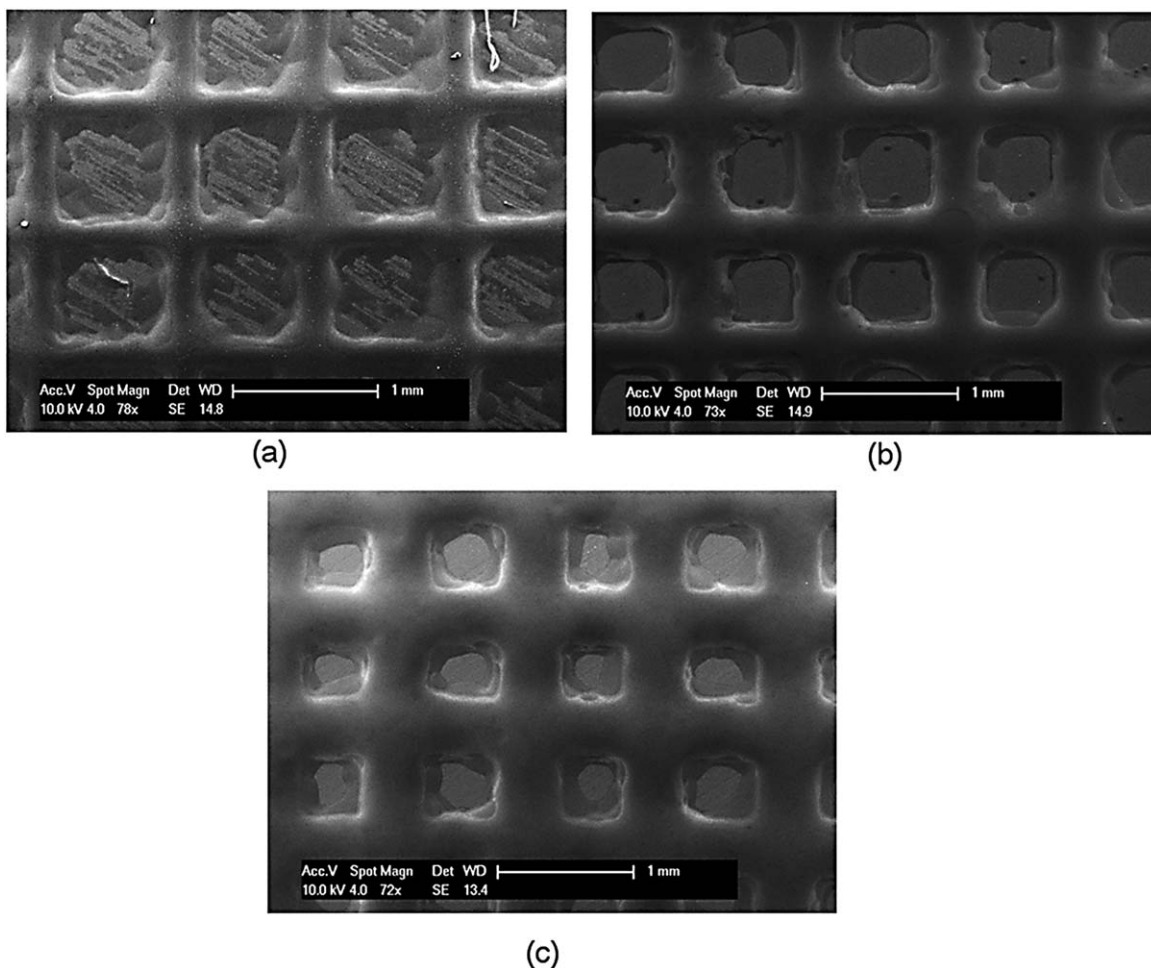


FIGURE 12. SEM pictures of printed mesh structure with different wall thickness: (a) 150 μm, (b) 300 μm, and (c) 500 μm.

during the manufacture process. This suggests that significant numbers of photons were not penetrating to layers below. With the second stage of illumination, even with the high intensity of illumination, there was no significant increase in modulus observed on the bottom layer, and thus, one may assume that in this case, few photons were able to penetrate to this depth (Figure 18). This was further confirmed by the measurement of the absorbance spectrum (Figures 5 and 6).

The samples printed in air with lower PI concentration showed more spreading (rounded edge) than those with high PI concentrations or printed in nitrogen environment. The likely cause of this is that the curing speed of the ink with 1 Wt % PI and AC is slower in air, allowing the droplet to continue spreading and possibly be unable to support drops deposited on it sufficiently well to create sharp edges. Higher PI and acceleration concentration will generate more excited PI-free radicals when illuminated by UV light as well as more excited ACs to protect the reaction from being inhibited by the oxygen in the environment, both of which will accelerate the cross-linking procedure. In principle, if each droplet can become fully cured as soon as it is deposited, they should be able to stack up (Figure 19).

However, when there was insufficient curing, the droplets may only be partially cured before the other drops were coincident. This effect will be amplified further when the next drop is placed on top, as the partial curing will mean the low viscosity drop will “sag” and slide down the edge of the previous drop due to gravitational and spreading effects. This caused irregular and rounded edges [e.g., Figure 7(a,b)]. As the curing speed increases, the deposited drops will be more viscous and less mobile, creating a situation where edges will be sharper and less susceptible to spreading effects [Figure 7(c-f)]. This hypothesis was verified using FTIR analysis (Figure 10) where the characteristic peak at 810 cm^{-1} was used to track the conversion of the double bond.^{48,49} Figure 10(b) shows the normalized peak height at 810 cm^{-1} for each sample, and it can be seen that the intensity of the characteristic peak at 810 cm^{-1} decreased as the PI concentration increased, indicating more conversion of the C=C double bond and higher levels of curing for samples printed in air with higher initiator concentration.

This is because the higher initiator concentration will generate more excited free radicals at the initiation stage, which largely increases the chance that excited free radicals meet an oligomer and enter the chain propagation stage. This, therefore,

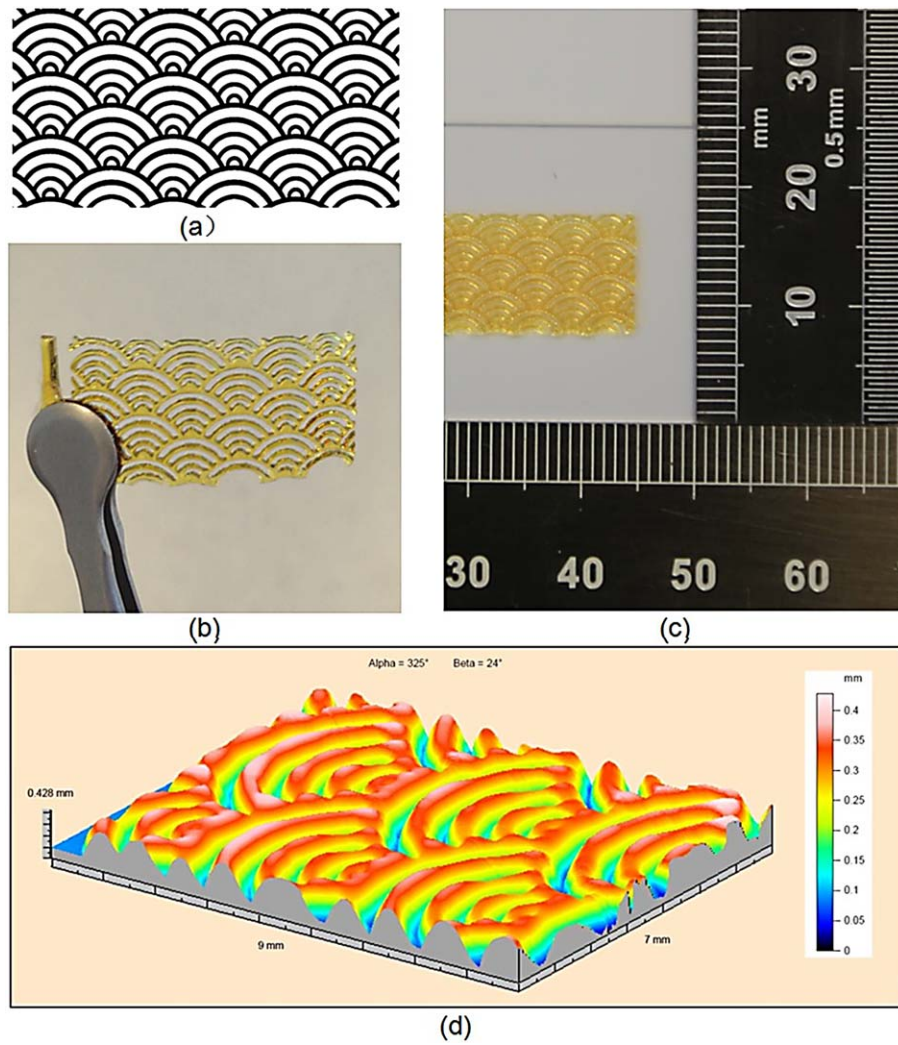


FIGURE 13. Curving mesh structure printing: (a) printing pattern, (b) sample appearance after taking off from glass slide, (c) top view of printed sample, and (d) surface profiling of printed curving mesh structure.

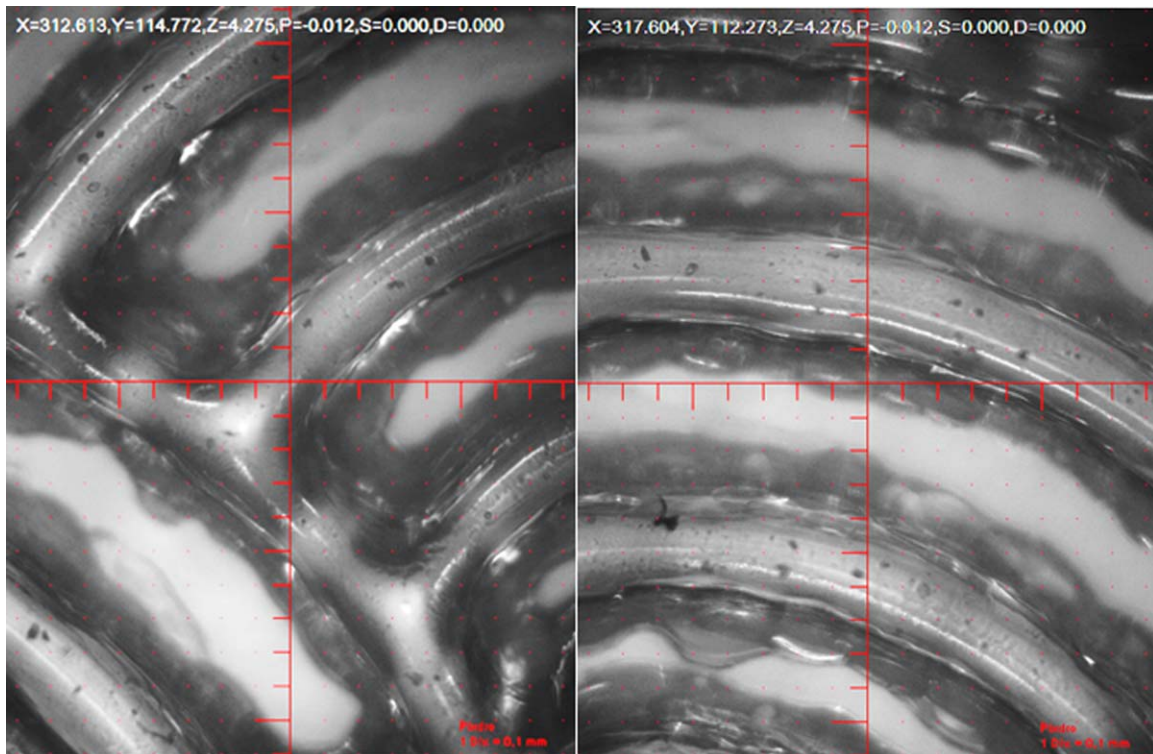


FIGURE 14. Microscopy pictures of printed curving mesh (1 division = 100 μm).

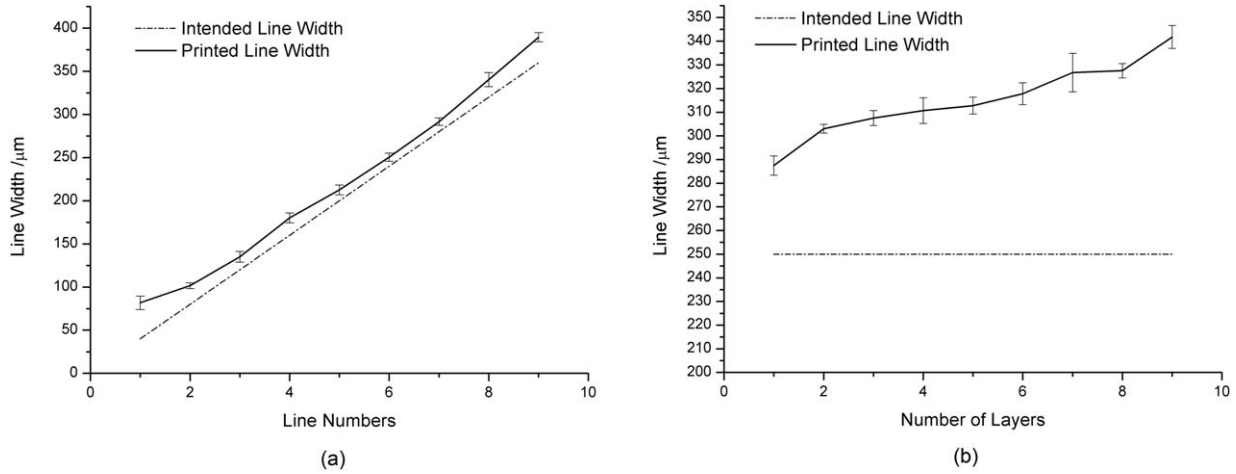


FIGURE 15. (a) Comparison of printed line width with intended line width in the designed pattern. (b) Line width increment with the increase in the number of printed layers. Data presented as mean ± standard error ($n = 5$).

can accelerate the cross-link reaction in a less favorable environment, e.g., top surface of the sample printed in air (oxygen inhibition and less UV illumination due to no subsequent layers deposited on top and, therefore, no further passes of the UV) as many backup excited initiators were generated. This assumes that an improved curing speed at the top surface would be achieved for the samples with higher initiator concentration and printed in air environment. However, in the chain propagation stage, a high concentration of excited oligomer chains will also have a greater chance to meet another excited oligomer and terminate. This will lead to more premature polymer chains being terminated, which reduces the cross-link density of the whole network. Therefore, a sample with lower cross-link density (higher initiator concentrations) will manifest lower hardness and modulus. Moreover, higher PI concentration also means that more uncross-linkable reactants were introduced that lead to a lower cross-link density also. Similar effects have been reported^{50,51} where excessive PI concentrations reduced the modulus of cured samples. Similarly, Naka-

jima et al.⁵² observed that excessive initiator concentration led to the formation of dangling chains, which caused a reduction in modulus.

It was also observed from Figure 8 that on the bottom surface, inks with lower PI and AC concentrations manifest higher hardness and modulus. This may indicate that if the sample was properly cured, the samples with lower PI and AC concentrations will possess higher hardness and modulus values. A similar phenomenon was also observed for the samples printed in a nitrogen environment, as shown in Figure 9, but this time on both the top and bottom surfaces. This gave further strength to the hypothesis that when the samples can achieve sufficient curing, the sample with the lower PI and AC concentrations will manifest greater hardness and modulus.

The ink was shown to be biocompatible both by direct contact with the cells and also upon exposure of the cells to media containing any chemicals that may have leached from the printed. PEGDA is added as a diluent but is not generally

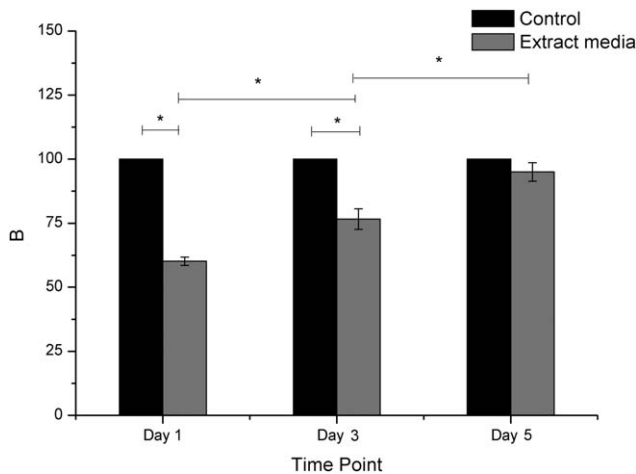


FIGURE 16. Metabolic activity of 3T3s cultured in extract media compared to the control. Data presented as mean ± standard error ($n = 5$). No statistical differences were found at day 5 between sample extract media and the control ($*p < 0.05$).

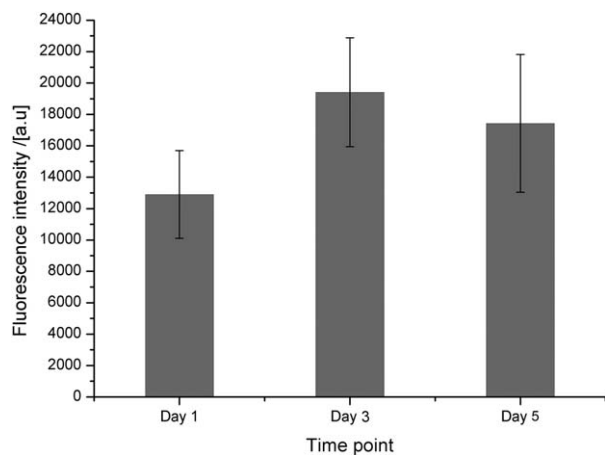


FIGURE 17. Metabolic activity of 3T3s seeded on scaffolds. Data presented as mean ± standard error ($n = 5$).

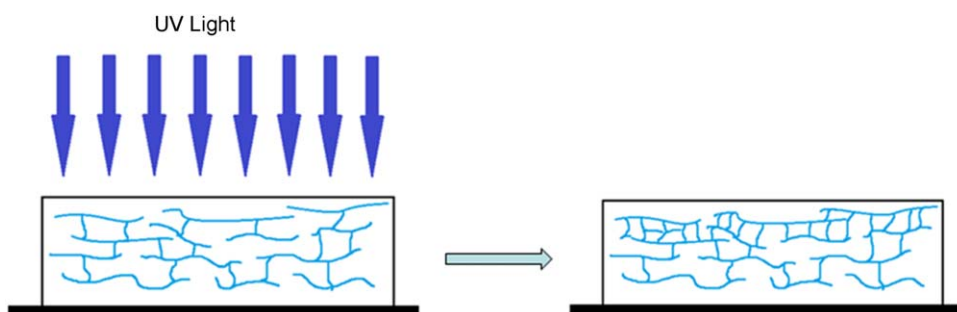


FIGURE 18. Schematic representation of the cross-linking of the internal polymer chains during postcuring.

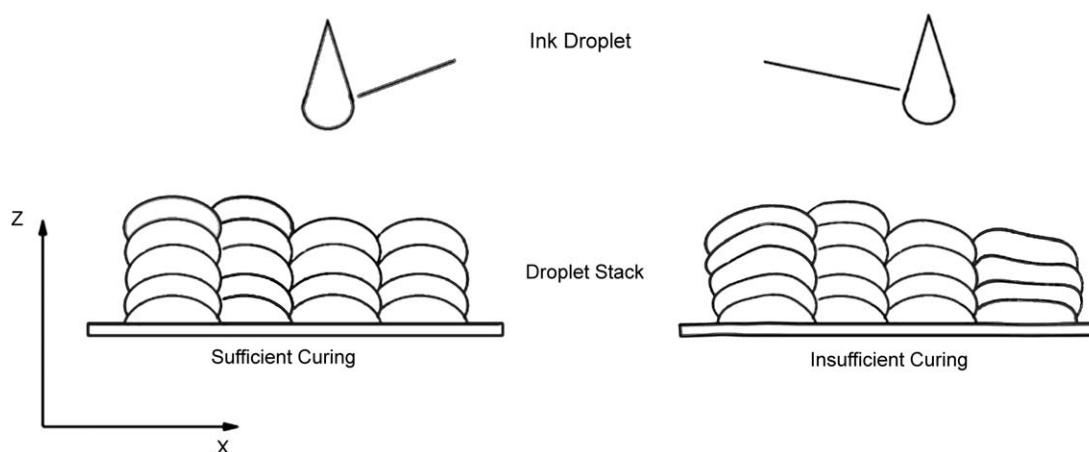


FIGURE 19. Schematic representation of deposited droplet in z-direction with different curing conditions.

considered easily degradable. However, the need for PEGDA can be minimized in the future through the use of alternative, higher temperature printhead units, leaving methacrylated PCL as the dominant component. Methacrylated PCL has previously been demonstrated to be degradable,²⁶ suggesting that in the future, the utility of products printed with this formulation may be extended to include biodegradable systems. Furthermore, the inherent scalability of ink jet printing, where printheads with numbers of nozzles in excess of 1024 are not uncommon, demonstrates the possibilities for ink jet-based manufacture of bespoke biomedical products.

CONCLUSIONS

A photocrosslinkable PCL-based ink that is suitable for 3D inkjet printing to produce biocompatible 3D structures has been demonstrated for the first time. In this article, PCLDMA: PEGDA (70:30) was chosen and observed to be printable from a Dimatix DMP-2830 at 60°C. The prepared ink could be cured sufficiently to retain structures during printing, and stable products were produced. Differences in hardness and modulus on the printed sample's top and bottom surfaces were observed. Both hardness and indentation modulus increased when postcuring was applied, but only the mechanical properties at the directly illuminated surface were improved as the UV light could not penetrate through the whole sample. The sample printed in an air environment had a hardness of

~4 MPa and a modulus of ~40 MPa, while those printed in a nitrogen environment had a hardness ~6 MPa and a modulus ~65 MPa, suggesting that optimization of the printing and curing processes may offer some degree of enhancement in the material properties. The developed ink also showed good biocompatibility with living mammalian cells in a cytotoxicity test, suggesting possible uses in the biomedical field.

ACKNOWLEDGMENTS

The authors would like to acknowledge funding support from University of Nottingham, the EPSRC (Grant number EP/1033335/2, EPSRC Centre for Innovative Manufacturing in Additive Manufacturing) and Loughborough University. Elisabetta Prina was funded by the EPSRC and MRC Centre for Doctoral Training in Regenerative Medicine (EP/L015072/1).

REFERENCES

1. Wang Y, Rodriguez-Perez MA, Reis RL, Mano JF. Thermal and thermomechanical behaviour of polycaprolactone and starch/polycaprolactone blend for biomedical applications. *Macromol Mater Eng* 2005;290:792–801.
2. Kulkarni RK, Moore EG, Hegyeli AF, Leonard F. Biodegradable poly (lactic acid) polymers. *J Biomed Mater Res* 1971;5:169–181.
3. Lasprilla AJR, Martinez GAR, Lunelli BH, Jardini AL, Filho RM. Poly-lactic acid synthesis for application in biomedical devices—A review. *Biotechnol Adv* 2012;30:321–328.
4. Ramanath HS, Chua CK, Leong KF, Shah KD. Melt flow behaviour of poly-ε-caprolactone in fused deposition modelling. *J Mater Sci* 2008;19:2541–2550.

5. Pitt CG, Schinder A, Capronor. A biodegradable delivery system for levonorgestrel, long-acting contraceptive systems, Philadelphia. Harpen Row 1984:48–63.
6. Middleton JC, Tipton AJ. Synthetic biodegradable polymers as orthopedic devices. *Biomaterials* 2000;21:2335–2346.
7. Briegerv D, Topol E. Local drug delivery systems and prevention of restenosis. *Cardiovasc Res* 1997;35:405–413.
8. Bertrand OF, Sipehia R, Mongrain R, Rodes J, Tardif J, Bilodeau L, Cote G, Bourassa MG. Biocompatibility aspects of new stent technology. *J Am Coll Cardiol* 1998;32:562–571.
9. Eberhart RC, Su SH, Nguyen KT, Zilberman M, Tang L, Nelson KD, Frenkel P. Review: Bioresorbable polymeric stents: current status and future promise. *J Biomater Sci Polym Ed* 2003;14:299–312.
10. ASTM. F2792 standard terminology for additive manufacturing technology, 2012, available at: <http://www.astm.org> (Date of access:28/04/2016).
11. Hague R, Campbell I, Dickens P. Implications on design of rapid manufacturing. *Proc Inst Mech Eng C: J Mech Eng Sci* 2003;217:25–30.
12. Jiang C, Huang F, Hsieh M. Fabrication of synthesized PCL-PEG-PCL tissue engineering scaffolds using an air pressure-aided deposition system. *Rapid Prototyping J* 2011;17:288–297.
13. Williams JM, Adewumi A, Schek RM, Flanagan CL. Bone tissue engineering using polycaprolactone scaffold fabricated via selective laser sintering. *Biomaterials* 2005;26:4817–4827.
14. Eshraghi S, Das S. Mechanical and microstructural properties of polycaprolactone scaffolds with one-dimensional, two-dimensional and three-dimensional orthogonally oriented porous architectures produced by selective laser sintering. *Acta Biomater* 2010;6:2467–2476.
15. Mannoos MS, Jiang Z, James T, Kong YL, Malatesta KA, Soboyejo WO, Verma N, Gracias DH, Mcalpine MC. 3D printed bionic ears. *Nano Lett* 2013;13:2634–2639.
16. Rengier F, Mehndiratta A, von Tengg-Kobligk H, Zechmann CM, Unterhinninghofen R, Kauczor HU, Giesel FL. 3D printing based on imaging data: Review of medical applications. *Int J Comput Assist Radiol Surg* 2010;5:335–341.
17. D'Urso PS, Effeney DJ, Earwaker WJ, Barker TM, Redmond MJ, Thompson RG, Tomlinson FH. Custom cranioplasty using stereolithography and acrylic. *Br J Plast Surg* 2000;53:200–204.
18. Singare S, Liu Y, Li D, Lu B, Wang J, He S. Individually prefabricated prosthesis for maxilla reconstruction. *J Prosthodont* 2007, doi: 10.1111/j.1532-849X.2007.00266.x
19. Harrysson OLA, Hosni YA, Nayfeh JF. Custom-designed orthopedic implants evaluated using finite element analysis of patient-specific computed tomography data: Femoral-component case study. *BMC Musculoskeletal Disord* 2007;8:91–100.
20. van Eeden SP, Ripamonti U. Bone differentiation in porous hydroxyapatite in baboons is regulated by the geometry of the substratum: Implications for reconstructive craniofacial surgery. *Plast Reconstr Surg* 1994;93:959–966.
21. Kujala S, Ryhänen J, Danilov A, Tuukkanen J. Effect of porosity on the osteointegration and bone ingrowth of a weight-bearing nickel-titanium bone graft substitute. *Biomaterials* 2003;24:4691–4697.
22. Elomaa L, Teixeira S, Hakala R, Korhonen H, Grijpma DW, Seppala JV. Preparation of poly(ϵ -caprolactone)-based tissue engineering scaffolds by stereolithography. *Acta Biomater* 2011;7(11):3850–3856.
23. Matsuda T, Mizutani M. Liquid acrylate-encapped biodegradable poly(ϵ -caprolactone-co-trimethylene carbonate). II. Computer-aided stereolithographic microarchitectural surface photoconstructs. *J Biomed Mater Res A* 2002;62(3):395–403.
24. He Y, Wildman R, Tuck C, Christie SDR, Edmondson S. An investigation of the behavior of solvent based polycaprolactone ink for material jetting. *Sci Rep* 2016, doi:10.1038/srep20852
25. Zhang F, Tuck C, Hague R, He Y, Saleh E, Li Y, Sturgess C, Wildman R. Inkjet printing of polyimide insulators for the 3D printing of dielectric materials for microelectronic applications. *J Appl Polym Sci* 2016;133(18):1–11.
26. Krober P, Delaney JT, Perelaer J, Schubert US. Reactive inkjet printing of polyurethanes. *J Mater Chem* 2009,19:5234–5238.
27. Hart LR, Harries JL, Greenland BW, Colquhoun HM, Hayes W. Supramolecular approach to new inkjet printing inks. *Appl Mater Interfaces* 2015;7(16):8906–8914.
28. Gunasekera DHAT, Kuek S, Hasanaj D, He Y, Tuck C, Croft A, Wildman RD. Three dimensional inkjet printing of biomaterials using ionic liquids and co-solvents. *Faraday Discuss* 2016, doi: 10.1039/C5FD00219B
29. Ibrahim M, Otsubo T, Narahara H, Koresawa H, Suzuki H. Inkjet printing resolution study for multi-material rapid prototyping. *JSME Int J Ser C* 2006;49:353–360.
30. Decker C. UV-radiation curing chemistry. *Pigm Resin Technol* 2001;30:278–286.
31. Feng Z, Sanping Z. Synthesis and characterization of biodegradable hydrogels based on photopolymerizable acrylate-terminated CL-PEG-CL macromers with supramolecular assemblies of acyclodextrins. *Polymer* 2003;44:5177–5186.
32. Park J, Woo DG, Sun BK, Chung HM. In vitro and in vivo test of PEG/PCL-based hydrogel scaffold for cell delivery application. *J Controlled Release* 2007;124:51–59.
33. Kweon HY, Yoo MK, Park IK, Kim TH, Lee HC, Lee HS. A novel degradable polycaprolactone networks for tissue engineering. *Biomaterials* 2003;24:801–808.
34. Malda J, Visser J, Melchels FP, Jüngst T, Hennink WE, Dhert WJA, Groll J, Huttmacher DW. 25th anniversary article: Engineering hydrogels for biofabrication. *Adv Mater* 2013;36:5011–5028.
35. Calvert P. Inkjet printing for materials and devices. *Chem Mater* 2001;23:3299–3305.
36. Decker C, Viet TNT, Decker D, Weber-Koehl E, UV-radiation curing of acrylate/epoxide systems. *Polymer* 2001;42:5531–5541.
37. Ferreira P, Coelho JFJ, Gil MH. Development of a new photocrosslinkable biodegradable bioadhesive. *Int J Pharm* 2008;352:172–181.
38. Cuchiara PC, Allen AB, Chen TM, Miller JS, West JL. Multilayer microfluidic PEGDA hydrogels. *Biomaterials* 2010;31:5491–5497.
39. Hahn MS, Taite LJ, Moon JJ, Rowland MC, Ruffino KA, West JL. Photolithographic patterning of polyethylene glycol hydrogels. *Biomaterials* 2006;27:2519–2524.
40. Hahn MS, Miller JS, West JL. Laser scanning lithography for surface micropatterning on hydrogel. *Adv Mater* 2005;17:2939–2942.
41. Huang MH, Huttmacher DW, Schantz J, Vacanti CA, Braud C, Vert M. Degradation and cell culture studies on block copolymers prepared by ring opening polymerization of ϵ -caprolactone in the presence of poly(ethylene glycol). *J Biomed Mater Res A*, 2004; 69A(3):417–427.
42. Jette KK, Law D, Schmitt EA, Kwon GS. Preparation and drug loading of poly(ethylene glycol)-block-poly(ϵ -caprolactone) micelles through the evaporation of cosolventazeotrope. *Pharm Res* 2004;21:1184–1191.
43. Studer K, Decker C, Beck E. Overcoming oxygen inhibition in UV-curing of acrylate coatings by carbon dioxide inerting, Part I. *Prog Org Coat* 2003;48:92–100.
44. Butler IB, Schoonen MAA, Rickard DT. Removal of dissolved oxygen from water: A comparison of four common techniques. *Talanta* 1994;41:211–215.
45. Chen X, Ashcroft IA, Wildman RD, Tuck CJ. An inverse method for determining the spatially resolved properties of viscoelastic-viscoplastic three-dimensional printed materials. *Proc Math Phys Eng Sci* 2015;471(2183):1–23.
46. Gardel ML, Shin JH, MacKintosh FC, Mahadevan L, Matsudaora P, Weitz DA. Elastic behaviour of cross-linked and bundled actin networks. *Science* 2004;304:1301–1305.
47. Coran AY. In: Eirich FR, editor. *Science and Technology of Rubber: Chapter 4 The Molecular Basis of Rubber like Elasticity*. New York: Academic Press; 1978, pp 292–293.
48. Xu J, Pang W, Shi W. Synthesis of UV-curable organic-inorganic hybrid urethane acrylates and properties of cured films. *Thin Solid Films* 2006;514:69–75.
49. Hong BT, Shin KS, Kim DS. Ultraviolet-curing behavior of an epoxy acrylate resin system. *J Appl Polym Sci* 2005;98:1180–1185.
50. Nakajima T, Furukawa H, Tanaka Y, Kurokawa T, Osada Y, Gong JP. True chemical structure of double network hydrogels. *Macromolecules* 2009;42:2184–2189.
51. Wang S, Yaszemski MJ, Gruetzmacher JA, Lu L. Photo-crosslinked poly(ϵ -caprolactone fumarate) networks: Roles of crystallinity and crosslinking density in determining mechanical properties. *Polymer* 2008;49:5692–5699.